JOURNAL

OF THE AMERICAN CHEMICAL SOCIETY

VOLUME 110, NUMBER 5 MARCH 2, 1988

Evidence for Static Localization in the Lowest Optically Excited States of Ruthenium(II) Diimine Complexes: A Solvent- and Time-Dependent Photoselection Study at 77 K

M. L. Myrick,† R. L. Blakley, M. K. DeArmond,*† and M. L. Arthur

Contribution from the Department of Chemistry, North Carolina State University, Raleigh, North Carolina 27695-8204. *Received April 13, 1987*

Abstract: The 77 K absorption, emission, steady-state excitation photoselection (SSExP), and time-resolved excitation photoselection (TRExP) results are reported for 11 $[Ru(L)_3](PF_6)_2$ complexes with 2,2′-diimine ligands (L). The ligands are 2,2′-bipyridine (bpy), 1,10-phenanthroline (phen), 2,2′-bipyrazine (bpz), 2-(2-pyridyl)quinoline (pq), and 2,2′-biquinoline (biq). Complexes of the form $[Ru(L)_3]^{2+}$ (L = bpy, phen, bpz, pq, and biq) were examined as well as mixed-ligand complexes of the form $[Ru(bpy)_n(L)_{3-n}]^{2+}$ (n = 1, 2) (L = phen, bpz, and pq). Data are also presented for the monomeric model complex, $[Ru(bpy)(py)_4]^{2+}$ (py = pyridine). Data indicate that optical excitation leads to static localization of the optically excited electron. A model is developed that rationalizes the maximum value obtainable in the SSExP data. Solvent effects observed in the TRExP data are explained in terms of relative rates of spin–lattice relaxation associated with different solvents.

The photoselection spectrum of $[Ru(bpy)_3]^{2+}$ (bpy = 2,2′-bipyridine) was first investigated by Fujita and Kobayashi, who discussed the data in terms of an excited-state molecule of D_3 symmetry, meaning the excited electron density was evenly distributed over all three ligands.[1] An anomaly existed in their data which was inconsistent with a D_3-symmetry excited state, and this prompted Carlin and DeArmond[2] to reinvestigate these data for the molecule. They showed that the emitting state of this complex must have a lower symmetry than D_3, such as C_2 or C_{2v}. This model suggested an excited complex of the form $[Ru(bpy)_2(bpy^*)]^{2+}$ in which the optical electron was localized on a single bpy or Ru–bpy chromophore. This latter argument was supported by excited-state resonance Raman data[3] and has since gained support from the transient absorption data[4] and time-resolved photoselection data.[5]

This paper is intended to show that other $[Ru(L)_3]^{2+}$ (L = α,α-diimine bidentate ligand) complexes exhibit the same photoselection properties as the bpy species and to extend this work to include mixed-ligand complexes. A solvent variation is made to further verify the intrinsic nature of the localization phenomenon. Also a model is developed based upon the number of emitting chromophores available in these molecules which rationalizes the photoselection data and allows general predictions to be made for the magnitude of the maximum in the steady-state photoselection spectrum.

Experimental Section

A. Materials and Synthesis. Spectroscopic grade methanol (MeOH), 2-propanol (2-prOH), and methylene chloride (CH_2Cl_2), anhydrous diethyl ether (Et_2O), and absolute ethanol (EtOH) were obtained from the Fisher Scientific Co. and used without further purification. The water used was deionized and distilled once. These solvents were examined for possible fluorescent impurities and none was found. Acetic anhydride (Ac_2O) was reagent grade. In addition to the alcoholic glasses, a binary mixture of methylene chloride and diethyl ether glasses in any CH_2Cl_2/Et_2O ratio of 2:1 or less and Ac_2O/Et_2O mixtures glasses in ratios of 5:2 or less were used. Both of these new glasses provide unique characteristics useful in characterizing the complexes under study.

Ethanol solutions of Coumarin 460 and Coumarin 481, provided by Exciton Corp., were used to obtain the necessary excitation wavelengths for the time-resolved data (vide infra). The complexes $[Ru(bpy)_n(pq)_{3-n}](PF_6)_2$ (n = 0, 1, 2) (where bpy is 2,2′-bipyridine and pq is 2-(2-pyridyl)quinoline) were available from previous studies,[6] as were the $[Ru(bpy)_n(bpz)_{3-n}](PF_6)_2$ (n = 0, 1, 2) complexes[7] and the $[Ru(biq)_3](ClO_4)_2$ complex.[8] The $[Ru(bpy)_n(phen)_{3-n}](PF_6)_2$ (n = 0, 1, 2, 3) complexes were made by using $RuCl_3 \cdot xH_2O$, 2,2′-bipyridine, and 1,10-phenanthroline (phen) from Fisher Scientific Co. Both ligands were recrystallized from MeOH prior to use. The n = 0 and n = 3 complexes were made by using the method of Palmer and Piper[9] and were recrystallized three times from MeOH/2-prOH mixtures. The n = 1 and n = 2 complexes were synthesized by first making the bis complexes, $[Ru(L)_2Cl_2] \cdot xH_2O$, using $RuCl_3 \cdot xH_2O$ and the appropriate ligand. $RuCl_3 \cdot xH_2O$ in EtOH was first reduced to the green stage with H_2(g)

† Present address: Department of Chemistry, New Mexico State University, Las Cruces, New Mexico 88003.

(1) Fujita, I.; Kobayashi, H. *Inorg. Chem.* **1973**, *12*(12), 2758.
(2) (a) Carlin, C. M.; DeArmond, M. K. *Chem. Phys. Lett.* **1982**, *89*, 297. (b) Carlin, C. M.; DeArmond, M. K. *Chem. Phys. Lett.* **1985**, *107*, 53.
(3) Dallinger, R. F.; Woodruff, W. H. *J. Am. Chem. Soc.* **1979**, *101*, 4391.
(4) Milder, S. J.; Gold, J. S.; Kliger, D. S. *J. Phys. Chem.* **1986**, *90*, 548.
(5) Myrick, M. L.; Blakley, R. L.; DeArmond, M. K. *J. Am. Chem. Soc.* **1987**, *109*, 2841.
(6) Tait, C. D.; Vess, T. M.; DeArmond, M. K.; Hanck, K. W.; Wertz, D. W. *J. Chem. Soc., Dalton Trans.*, in press.
(7) Gex, J. N.; DeArmond, M. K.; Hanck, K. W. *J. Phys. Chem.* **1987**, *91*, 251.
(8) Tait, C. D.; MacQueen, D. B.; Donohoe, R. J.; DeArmond, M. K.; Hanck, K. W.; Wertz, D. W. *J. Phys. Chem.* **1986**, *90*, 1766.
(9) Palmer, R. A.; Piper, T. S. *Inorg. Chem.* **1966**, *5*(5), 864.

0002-7863/88/1510-1325$01.50/0

to aid in the yield by removing Ru(IV) impurities, and then after a stoichiometric amount of the appropriate ligand was added, the solution was refluxed under N_2(g) for 8 h. These dark purple-black bis intermediates were carefully purified following the method of Bosnich and Dwyer.[10] Next, a stoichiometric amount of the odd ligand was added to an EtOH solution of the appropriate bis complex and refluxed under N_2(g) for 4 h, resulting in an orange-red solution. Approximately 5–7 mL of H_2O was then added, and the EtOH was distilled from the solution, leaving the chloride salt of the mixed-ligand tris complex in H_2O. A metathesis reaction to form the hexafluorophosphate salt of the complex was then performed by dropwise addition of a 20% solution of $NaPF_6$ until precipitation appeared complete. Complexes with this anion have been shown to be stable to photolysis.[11] The complex [Ru(bpy)(py)$_4$](PF$_6$)$_2$ (py = pyridine) was prepared by the method of Krause,[12] proceeding via the intermediate [Ru(bpy)Cl$_3$].[13] Upon precipitation of this complex by metathesis with $NaPF_6$(aq), the bright orange complex was dried and refrigerated for stability. Solutions of the complex were found to be extremely photosensitive at room temperature but appeared stable when frozen in glassy solution at 77 K. Care was taken to perform all measurements of this material soon after synthesis because a small thermal instability is also indicated. The fluid solutions were manipulated only in complete darkness or under weak illumination from a Kodak Safelight with Kodak filter no. 1A.

The purity of all the complexes was monitored by examining the emission spectrum of each, using two distinct excitation wavelengths. Only one emission profile for each complex was found. Emission photoselection (EmP) spectra also indicated that the complexes were pure since only one emitting oscillator was observed in each case.

B. Spectroscopic Measurements. Low-temperature (77 K) absorption spectra were done with a Cary 2300 spectrometer using an Oxford Instruments Model DN1704 cryostat.

Polarization data were obtained with a high-resolution photoselection spectrometer,[14] now interfaced with a Zenith 158 computer. For this work a Hanovia 450-W Xe lamp was used for excitation, and a Hammamatsu R955 photomultiplier tube (PMT) was used for detection. Emission spectra at 77 K were obtained with the previously described high-resolution spectrometer without the polarizing chopper in place; these data were not corrected for PMT or monochromator response.

A Princeton Applied Research (PAR) Model 162 boxcar averager (5-ns gate and digital storage with a Model 164 gated integrator), a Molectron DL-II tunable dye laser pumped by a Molectron Model UV-12 pulsed N_2(g) laser (pulsewidth = 5 ns), and a 3/4-m No. 1800 Czerny-Turner spectrometer (Spex Industries, Inc.) equipped with a Hammamatsu R955 PMT were used to obtain the 77 K time-resolved excitation photoselection (TRExP) data. Since the photoselection experiment is an emission technique, the excitation wavelength was at a much higher energy in all cases than the monitored emitting wavelength; but, to ensure the absence of any problems due to laser scatter, glass filters provided by the Optic Corp. were used on the emission monochromator. Blank and scattering samples were run and no scattered light was detected at the monitored emission wavelengths.

The TRExP experiment was conducted manually. The gate was positioned at the desired time after the laser pulse and polarizers were arranged so that vertically polarized light excited the sample and vertically polarized light was detected (90° to the excitation beam) by the emission monochromator. The intensity of the emission (I_{vv}) was recorded (using a strip chart recorder) for 30 s. At this time, the beam was blocked for 30 s (to obtain a base line) and the emission polarizer was changed so that horizontally polarized light was detected and again the emission intensity (now I_{vh}) was recorded. A minimum of 10 runs, I_{vv} (30 s)–block (30 s)–I_{vh} (30 s)–block (30 s), were obtained at each of the desired times after the laser pulses. Alternation in this way minimizes the effects of any bleaching of the sample or nonphotochemical hole burning with a narrow laser line, as well as the slow loss of dye laser efficiency due to use of a nonflowing dye cell arrangement.

The intensity measurements I_{hh} and I_{hv} were obtained so that the data could be corrected for monochromator polarization response.[15] These data were then used to calculate the degree of polarization[16] with eq 1.

$$P = \frac{I_{vv} - (I_{hv}/I_{hh})I_{vh}}{I_{vv} + (I_{hv}/I_{hh})I_{vh}} \quad (1)$$

(10) Bosnich, B.; Dwyer, F. P. *Aust. J. Chem.* **1966**, *16*, 2229.
(11) Durham, B.; Walsh, J. L.; Carter, C. L.; Meyer, T. J. *Inorg. Chem.* **1980**, *19*, 860.
(12) Krause, R. A. *Inorg. Chim. Acta* **1977**, *22*, 209.
(13) Krause, R. A. *Inorg. Chim. Acta* **1978**, *31*, 241.
(14) Carlin, C. M.; Hanck, K. W.; DeArmond, M. K. *Rev. Sci. Instrum.* **1981**, *52*, 137.
(15) Azumi, T.; McGlynn, S. P. *J. Chem. Phys.* **1962**, *37*(10), 2413.
(16) Albrecht, A. C. *J. Mol. Spectrosc.* **1961**, *6*, 84.

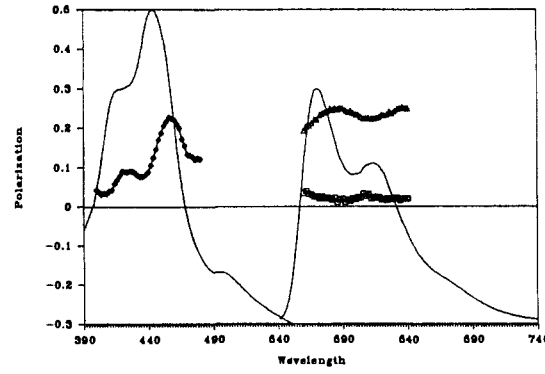

Figure 1. 77 K absorption and emission spectra of [Ru(bpz)$_3$](PF$_6$)$_2$ in EtOH. The SSExP spectrum (diamonds) is plotted across the absorption spectrum. Emission photoselection (EmP) spectra obtained by exciting 25 000 cm^{-1} (400 nm) (squares) and 21 900 cm^{-1} (456 nm) (triangles) are shown plotted across the emission spectrum.

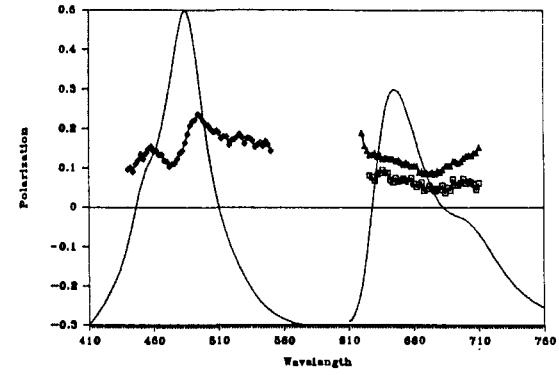

Figure 2. Absorption and emission spectra obtained at 77 K for [Ru(pq)$_3$](PF$_6$)$_2$ in 2:1 CH_2Cl_2/Et_2O. The SSExP spectrum (diamonds) is plotted across the absorption spectrum (monitored emission energy, 15 500 cm^{-1} (645 nm)). The EmP spectra plotted across the emission were obtained by exciting 23 300 cm^{-1} (430 nm) (squares) and 20 400 cm^{-1} (490 nm).

Results

Table I contains the position of the maximum of the charge-transfer (CT) absorption, the CT emission, the time-averaged (or steady state) excitation photoselection (SSExP), and the time-resolved excitation photoselection (TRExP, 0–5 and 300 ns) for a series of Ru(II) complexes in solvent systems of varying dielectric constant.

A. Tris Complexes of bpy, phen, bpz, pq, and biq. For tris-chelated complexes of the type [Ru(L)$_3$]$^{2+}$, the maximum SSExP value obtained in all cases (except biq; vide infra) is 0.22–0.24. A representative spectrum is given in Figure 1 and ref 2. In all cases the maximum in the SSExP was red-shifted 380–1500 cm^{-1} (most of the range 620 ± 70 cm^{-1}) from the CT absorption maximum (Figure 2). The Stokes shift of the emission showed a solvent dependence, with emission occurring at higher energy in the lowest dielectric constant (DC), weakest hydrogen-bonding (HB) solvent system. On a 0–5-ns time scale, the TRExP experiment shows a larger P_{max} value for these complexes. The increase of these TRExP values follows the increase of the dielectric constant and hydrogen-bonding ability of the solvent system used.

The complex [Ru(biq)$_3$](ClO$_4$)$_2$ (Figure 3) was studied in ethanolic solution and gave an SSExP maximum value of 0.37, which was 600 cm^{-1} red-shifted from the CT absorption maximum, but only 100 cm^{-1} red-shifted from a low-energy shoulder of the CT band. The emission for the complex occurred at 14 000 cm^{-1}, and no vibrational shoulder was observed, perhaps because of PMT sensitivity.

B. Mixed-Ligand Complexes. The [Ru(bpy)(L)$_2$]$^{2+}$ (L = pq, bpz) mixed-ligand complexes, in which the MLCT emission is associated with the Ru–L unit, have maximum SSExP values of

Table I. 77 K Energy Maxima ($\times 10^3$ cm^{-1}) for Various Spectroscopic Data[a] and the Excitation Photoselection Maxima in Various Solvent Systems

complex/solvent	Abs_{max}	Em_{max}	$SSExP_{max}$[b] position	$SSExP_{max}$[b] P_{max}	$TRExP_{max}$[c] 0–5 ns	$TRExP_{max}$[c] 300 ns
$[Ru(bpy)(py)_4]^{2+}$						
EtOH	21.4	17.1	21.1	0.43	0.43 ± 0.3	
$[Ru(bpy)_3]^{2+}$						
4:1 $MeOH/H_2O$	22.0	17.3	21.4	0.23	0.37 ± 0.04	0.20 ± 0.02
EtOH	22.0	17.4	21.4	0.23	0.30 ± 0.04	0.20 ± 0.02
2:1 CH_2Cl_2/Et_2O	22.0	17.6	21.4	0.23	0.24 ± 0.02	0.20 ± 0.02
$[Ru(phen)_3]^{2+}$						
4:1 $MeOH/H_2O$	22.3	17.8	21.7	0.22	0.33 ± 0.02	0.23 ± 0.02
EtOH	22.3	17.9	21.7	0.23	0.32 ± 0.07	0.22 ± 0.03
2:1 CH_2Cl_2/Et_2O	22.2	18.0	21.6	0.23	0.22 ± 0.03	0.20 ± 0.02
$[Ru(bpz)_3]^{2+}$						
4:1 $MeOH/H_2O$	22.5	17.5	21.9	0.25	0.34 ± 0.04	0.26 ± 0.02
EtOH	22.5	17.5	21.9	0.23	0.20 ± 0.02	0.20 ± 0.02
2:1 CH_2Cl_2/Et_2O	*d*	*d*	*d*	*d*	*d*	*d*
$[Ru(pq)_3]^{2+}$						
4:1 $MeOH/H_2O$	20.7	15.2	19.2	0.22	0.33 ± 0.05	0.20 ± 0.03
EtOH	20.7	15.2	19.2	0.23	0.28 ± 0.04	0.22 ± 0.03
2:1 CH_2Cl_2/Et_2O	20.6	15.5	20.2	0.24	*d*	*d*
$[Ru(biq)_3]^{2+}$						
EtOH	18.5	14.0	17.9	0.38		
$[Ru(bpy)_2(phen)]^{2+}$						
4:1 $MeOH/H_2O$	22.2	17.5	21.5	0.23		
EtOH	22.2	17.5	21.	0.23	0.43 ± 0.06	0.20 ± 0.02
2:1 CH_2Cl_2/Et_2O	22.1	17.6	21.4	0.23		
$[Ru(bpy)(phen)_2]^{2+}$						
4:1 $MeOH/H_2O$	22.2	17.5	21.6	0.21		
EtOH	22.2	17.5	21.5	0.24	0.44 ± 0.04	0.21 ± 0.03
2:1 CH_2Cl_2/Et_2O	22.1	17.9	21.5	0.21		
$[Ru(bpy)_2(bpz)]^{2+}$						
4:1 $MeOH/H_2O$	21.0	15.3	20.4	0.39		
EtOH	21.0	15.6	20.6	0.43		
2:1 CH_2Cl_2/Et_2O	*d*	*d*	*d*			
$[Ru(bpy)(bpz)_2]^{2+}$						
4:1 $MeOH/H_2O$	21.6	17.5	21.9	0.32		
EtOH	21.6	17.5	21.9	0.34	0.41 ± 0.05	0.33 ± 0.06
2:1 CH_2Cl_2/Et_2O	*d*	*d*	*d*			
$[Ru(bpy)_2(pq)]^{2+}$						
4:1 EOH/H_2O	20.6	15.3	20.3	0.40		
EtOH	20.6	15.3	20.1	0.42		
2:1 CH_2Cl_2/Et_2O	20.7	15.6	20.2	0.39		
$[Ru(bpy)(pq)_2]^{2+}$						
4:1 $MeOH/H_2O$	20.5	15.3	20.2	0.34		
EtOH	20.5	15.3	20.2	0.33	0.41 ± 0.06	0.31 ± 0.05
2:1 CH_2Cl_2/Et_2O	20.5	15.5	20.3	0.33		

[a] Abs = absorption, Em = emission, SSExP = steady-state excitation photoselection, and TRExP = time-resolved excitation photoselection. [b] The position and value of the steady-state excitation photoselection maximum obtained by monitoring at the emission maximum. [c] The time-resolved excitation photoselection value at 0–5 and 300 ns obtained by exciting into the SSExP maximum and monitoring at the emission maximum. [d] Values unobtainable due to solubility problems.

Table II. Angles (Deg) between Dimer and Monomer Axes (of Figure 12)

angle	value	angle	value	angle	value
Z,x	45	*X,x*	65.9	*Y,x*	125.3
Z,y	60	*X,y*	73.2	*Y,y*	35.3
Z,z	120	*X,z*	30	*Y,z*	90

0.33 and 0.34 (Table I and Figure 4), and these values are red-shifted 200–370 cm^{-1} from their absorption maxima. The TRExP data of these complexes show a higher value, 0.41, on the 0–5-ns time scale. In these complexes, both bpz and pq have a lower energy π^* orbital than does bpy, and therefore emission occurs from the Ru–bpz or the Ru–pq portion of the complexes.[17–19] The Stokes shift in the emission increases as the DC and HB ability of the solvent increases.

In the complexes $[Ru(bpy)_2(L)]^{2+}$ (L = pq, bpz), where L is involved in the CT emission, SSExP values of 0.43–0.39 (Table I and Figure 5) were obtained. These maximum values were red-shifted from the maximum of the CT absorption 380–500

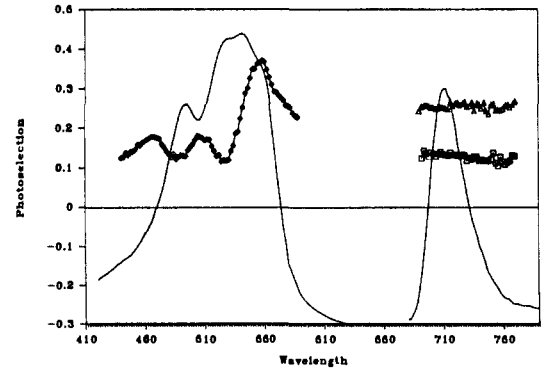

Figure 3. Absorption and emission spectra of $[Ru(biq)_3]^{2+}$ in EtOH at 77 K. Across the absorption is plotted the SSExP spectrum (diamonds) that is obtained by monitoring 14 000 cm^{-1} (712 nm) in the emission. Two EmP spectra are shown plotted across the emission, one obtained from exciting 18 500 cm^{-1} (540 nm) (triangles), the other from exciting 20 800 cm^{-1} (480 nm).

(17) Rillema, D. P.; Allen, G.; Meyer, T. J.; Conrad, D. *Inorg. Chem.* **1983**, *22*(11), 1617.
(18) Klassen, D. M. *Chem. Phys. Lett.* **1982**, *93*(4), 383.
(19) Anderson, S.; Seddon, K. R.; Wright, R. D. *Chem. Phys. Lett.* **1980**, *71*(2), 220.

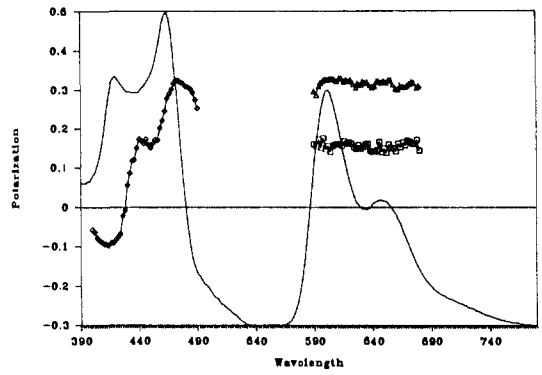

Figure 4. Absorption and emission spectra for $[Ru(bpy)(bpz)_2](PF_6)_2$ at 77 K in EtOH. Plotted across the absorption spectrum is the SSExP spectrum (diamonds) obtained by monitoring 16 600 cm^{-1} (602 nm) in the emission. Across the emission spectrum is plotted the EmP spectra obtained by exciting 21 200 cm^{-1} (472 nm) (triangles) and 22 700 cm^{-1} (440 nm) (squares).

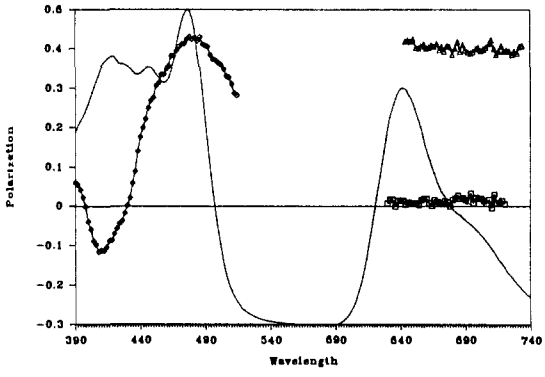

Figure 5. 77 K absorption and emission spectra for $[Ru(bpy)_2(bpz)](PF_6)_2$ in EtOH. The SSExP spectrum (diamonds) is shown plotted across the absorption spectrum (monitored emission energy, 15 600 cm^{-1} (641 nm)). Two EmP spectra are shown plotted across the emission spectrum, one by exciting 23 400 cm^{-1} (428 nm) (squares), the other by exciting 20 800 cm^{-1} (480 nm) (triangles).

cm^{-1}. The TRExP experiment was not attempted on these complexes since their maximum P values were already near the maximum theoretical level ($P = 0.5$).[16] As previously stated, the emitting level for these complexes lies on the L portion of the complex. The Stokes shift for these complexes increases as the DC and the HB ability of the solvent was increased.

The complex $[Ru(bpy)(py)_4]^{2+}$ exhibited a more simple photoselection spectrum (Figure 6) with a P_{max} of 0.43, near the theoretical linear–linear limit. In this complex, bipyridine has the lowest energy π^* orbital, and the Ru–bpy chromophore is the expected origin of the luminescence. The spectrum is slightly complicated by the presence of a strong band to higher energy, assigned as MLCT to pyridine, which obviously exhibits negative polarization. However, it is apparent that across most of the MLCT to bipyridine a photoselection value near the theoretical limit is attained. This is confirmed by preliminary evidence obtained in this laboratory for the mono-bpy complex $[Ru(bpy)(CN)_4]^{2-}$, which gives photoselection data very similar to those of $[Ru(bpy)(py)_4]^{2+}$. The absorption profile of the MLCT to bipyridine, shown in Figure 6, is very similar to that of $[Ru(bpy)_3]^{2+}$, as is the profile of the luminescence. No time dependence of the photoselection value at the maximum is found.

Previous studies[20] indicated the emission properties of the Ru–bpy chromophore and the Ru–phen chromophore were so similar that the $[Ru(bpy)_n(phen)_{3-n}]^{2+}$ ($n = 1, 2$) complexes could not be distinguished from the $[Ru(L)_3]^{2+}$ (L = bpy, or phen) complexes. Since $[Rh(bpy)_n(phen)_{3-n}]^{3+}$ ($n = 1, 2$) complexes exhibit a dual emission,[21] a dual emission might be expected from

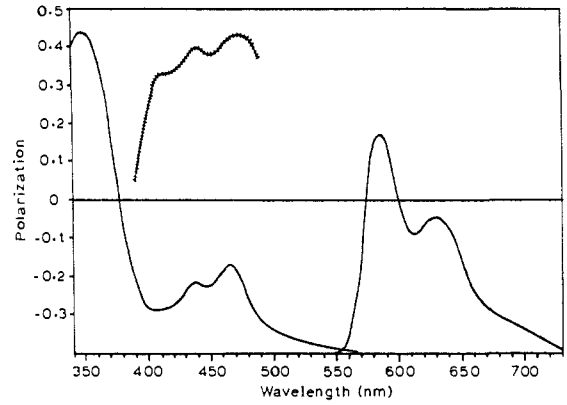

Figure 6. Absorption and emission spectra for $[Ru(bpy)(py)_4]^{2+}$ in EtOH at 77 K. Plotted across the absorption spectrum is the SSExP (crossed line) obtained by monitoring 17 100 cm^{-1} (585 nm) in the emission.

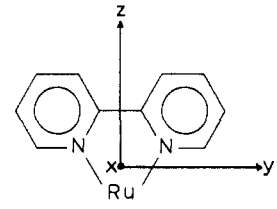

Figure 7. Axis system of monomer unit.

the Ru analogues; but due to the similarities of the two chromophores, no dual emission has been previously detected. The SSExP data for the mixed-ligand bpy/phen complexes are unusual since the profile is identical with that obtained for the $[Ru(L)_3]^{2+}$ (L = bpy, phen) complexes, with maximum values of 0.21–0.24. The red shift between the CT absorption maximum and the SSExP maximum was 620–790 cm^{-1}. The TRExP showed P_{max} values of 0.44–0.43 (in the 0–5 ns time scale). As for the other complexes, the Stokes shift in the emission increased as the DC and HB properties of the solvent increased.

Discussion

A. The Monomeric Complex, $[Ru(bpy)(py)_4]^{2+}$. Albrecht's photoselection theory[16] predicts that molecules with linear oscillators should have a theoretical SSExP limiting value of either $+^1/_2$ or $-^1/_3$, depending upon whether the oscillators are parallel or oriented at right angles to one another, implying that the total symmetries of the transitions are different. In the event of degeneracies, other values are possible. For planar absorption, planar emission a value of $+^1/_7$ is possible, but in the C_{2v} molecule $[Ru(bpy)(py)_4]^{2+}$ we need only be concerned with the limiting values for linear oscillators.

The fact that a relatively featureless photoselection profile, lowered at high energy by the intense, negatively polarized MLCT-py band, is measured across most of the MLCT band involving bipyridine has several implications. The first is that the oscillators for absorption and emission are oriented parallel to one another for absorption through this region. We further conclude that most CT oscillator strength across this band is polarized along a single axis of the monomer unit. This axis is presumably the z axis of the monomer as depicted in Figure 7 based upon identification of the transition as being of charge-transfer origin.

In addition, we make several conclusions about the nature of the lowest lying triplet state in this complex.

A triplet state in C_{2v} symmetry is comprised of three sublevels with different total symmetries. Since only a single linear oscillator is indicated in emission at 77 K, it is apparent that only a single sublevel achieves significant luminescent character via spin–orbit coupling to higher energy spin-allowed transitions.

Also, as found earlier,[22] in the C_{2v} point group spin–orbit coupling cannot connect singlet and triplet states derived from

(20) Crosby, G. A.; Elfring, W. H., Jr. *J. Am. Chem. Soc.* **1976**, *80*, 2206.

(21) DeArmond, M. K.; Carlin, C. M. *Coord. Chem. Rev.* **1981**, *36*, 325.

(22) Kober, E. M.; Meyer, T. J. *Inorg. Chem.* **1984**, *23*, 3877.

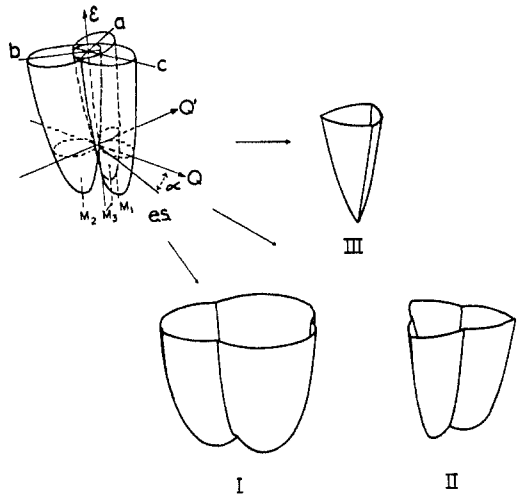

Figure 8. Three surfaces formed from intersection of potential energy wells of $[Ru(L)_3]^{2+}$ species with small exciton interaction. The lowest surface, I, has three minima. The central surface, II, has three shallow minima. The upper surface, III, has a single minimum.

identical orbital occupancies. Using the assumption that the singlet–triplet splitting is similar for each of the three possible CT states involving the lowest π^* orbital of bipyridine, we infer that the lowest singlet transition has a very small oscillator strength for its 0–0 band.

B. Tris Complexes of bpy, phen, bpz, pq, and biq. In previous photoselection studies[2,5] and other references,[3,4] $[Ru(bpy)_3]^{2+}$ has been shown to have a C_2 or C_{2v} emitting excited state of the form $[Ru(bpy)_2(bpy^*)]^{2+}$. The single-ring emitting state[2] of this complex leads to the treatment of the molecule as a trimer with three essentially noninteracting Ru–bpy chromophores. Figure 8 shows three nondegenerate spatially distinct excited states for the complex. Each state belongs to a separate Ru–bpy unit, and each is a valence isomer of the others. Very weak exciton coupling[23] of these three states produces three unique surfaces, the lowest of which possesses three minima corresponding to localized states of the trimer, as shown in Figure 8. The three surfaces shown in Figure 8 are equivalent to the surfaces proposed by Braterman et al.[24]

The discussion above has centered upon the C_2 or C_{2v} description of the excited states of these "trimer" complexes, so photoselection of these complexes should also yield limiting values of $+^1/_2$ or $-^1/_3$. The experimental SSExP values exhibited by these complexes at 77 K do not approach these limits, possessing maximum values of 0.23 (except biq; vide infra). However, this does not imply delocalization and D_3 symmetry, because the maximum values obtained exceed $^1/_7$, the maximum possible for involvement of a planar oscillator.

Overlapping electronic bands[16] in the absorption spectrum with different polarizations would result in mixed polarizations, resulting in lowered photoselection values, but this seems unlikely in these cases since the maximum value obtained is red-shifted 650 cm^{-1} from the CT absorption maximum. This shift is also present in molecules with $SSExP_{max}$ values equal to 0.43 (Table I), verifying little effect from overlapping bands. Rotation of the molecule subsequent to excitation can randomize photoselection data, resulting in lowered values,[25] but true rotation of the molecules can be eliminated since they are in a rigid frozen matrix. Excited-state intermolecular energy transfer also can lower $SSExP_{max}$ values, but this is unlikely since all of the solutions were 10^{-4} M, which means the solute molecules were separated by $\sim 10^4$ pm, and the solvent molecules do not have appropriate energy states to facilitate the energy transfer. Some researchers[26] have suggested that unsymmetrical interactions of the molecule with polar solvent environments could lower the symmetry of the excited state, a "red edge" effect. But exactly the same SSExP data are obtained in 2:1 CH_2Cl_2/Et_2O as in the alcohol and water/alcohol mixtures. Therefore, if these effects do exist, they are of minimal importance. It is true that in the 2:1 CH_2Cl_2/Et_2O system, ion-pairing effects could be important. Data for the hexafluorophosphate, perchlorate, and chloride salts of $[Ru(bpy)_3]^{2+}$ in the ion-pairing solvent 5:2 Ac_2O/Et_2O have been measured and no difference in the SSExP profile was observed.

The electrochemically reduced complex $[Ru(bpy)_2(bpy)^-]^+$ has been used to model the optically excited species, since in both cases an electron is localized on a single bpy portion of the molecule. The reduced complex has shown temperature-dependent ESR line broadening, which has been explained as thermal motion or "hopping" of the redox electron between adjacent ligands.[27,28] An analogous exciton motion can be postulated to occur between the three minima of the lowest surface in the weak-coupling model and, indeed, was proposed earlier by this group[5] to explain results obtained in the TRExP experiment. However, significant evidence exists to argue against such an interpretation of the TRExP result.

Using Carlin's method[29] to determine the polarization expected of an excited complex in which the localized excitation has been randomized among three equivalent units, one may easily show that P_{max} for the tris-chelated complexes should equal 0.14. Furthermore, Carlin's temperature-dependent photoselection data in solvents of varying viscosity indicate that exciton hopping is a relatively high-temperature process, not occurring in rigid solvents.

That the time-dependent polarization seen in the TRExP experiment is not due to actual excitonic motion is suggested by the ESR of the reduced species, where activation energies of $\sim$900 cm^{-1} for the electron-hopping process are measured. Such a rapid depolarization as is seen in the TRExP of the tris chelates suggests a process occurring on a nanosecond time scale. Yet the electron "hopping" in the reduced species is expected to be several orders of magnitude slower than this at 77 K[27] due to the large activation energy.

We now recognize that this unique time-dependent polarization behavior derives not from thermal motion, but from equilibration of the magnetic levels of the triplet state by spin–lattice relaxation (SLR). This process is characterized by a mean lifetime, T_1^{SL}, which is responsible for lifetime broadening and saturation effects in ESR spectroscopy.

Examples of spin–lattice relaxation times in organic systems are available to demonstrate that SLR at 77 K is a measurable feature of many triplet systems.[30–33] For instance, Hirota[30] has performed time-resolved ESR upon species such as phthalazine dissolved in EtOH at 77 K, finding that SLR has not occurred even 400 ns after creation of the triplet population. Bourdel[33] has found that T_1^{SL} for dilute deuteriophenanthrene in EtOH glass at 77 K is 230 ns.

The SLR mechanisms of Van Vleck[34] and Kronig[35] describe the interaction of the phonon spectrum of the "lattice" with the orbital angular momentum of unpaired electrons. This interaction is mediated by coupling of spin and orbital angular momenta (SOC). Therefore, SLR will be strongly affected by the extent of SOC present in the paramagnetic species, as well as the details

(23) Sinanoglu, O. *Modern Quantum Chemistry*; Academic: New York, 1965; pp 93–175.
(24) Braterman, P. S.; Heath, G. A.; Yellowlees, L. J. *J. Chem. Soc., Dalton Trans.* **1985**, 1081.
(25) Hercules, D. M. *Fluorescence and Phosphorescence Analysis*; Wiley: New York, 1966; pp 227–240.
(26) Yersin, H.; Gallhuber, E.; Hensler, G. *Chem. Phys. Lett.*, in press.
(27) Motten, A.; Hanck, K. W.; DeArmond, M. K. *Chem. Phys. Lett.* **1981**, *79*, 54.
(28) DeArmond, M. K.; Hanck, K. W.; Wertz, D. W. *Coord. Chem. Rev.* **1985**, *64*, 65.
(29) Carlin, C. M. Ph.D. Thesis, North Carolina State University, 1983.
(30) Terazima, M.; Yamauchi, S.; Hirota, N. *J. Chem. Phys.* **1985**, *83*, 3234.
(31) Yamauchi, S.; Hirota, N. *J. Phys. Chem.* **1984**, *88*, 4631.
(32) Bershon, M.; Baird, J. C. *An Introduction to Electron Paramagnetic Resonance*; W. A. Benjamin: New York, 1966; p 56.
(33) Lopez, P.; Bourdel, D.; Boujol, P.; Pescia, J. *Magnetic Resonance and Related Phenomena*; Allen, P. S., Andrew, E. R., Bates, C. A., Eds.; North-Holland: Amsterdam, 1975; p 423.
(34) Van Vleck, J. H. *Phys. Rev.* **1940**, *57*, 426.
(35) Kronig, R. *Physica* **1939**, *6*, 33.

of the phonon spectrum associated with the "lattice". Further, SLR will have a very large dependence upon T_b, the effective temperature of the phonon structure, normally taken to be the temperature of the surroundings.

The presence of the 4d metal, ruthenium, in the paramagnetic complexes being examined here will play some role in determining the efficiency of SLR processes in the triplet state, resulting in a relatively rapid SLR process. This is consistent with 5 ns or less values of T_1^{SL} as indicated by the TRExP experiment for some of these complexes. This is also in agreement with a result that no time dependence could be detected for the polarization of luminescence from $[Os(bpy)_3]^{2+}$ in identical circumstances,[36] indicating that the depolarization mechanism for this complex is more efficient than that for $[Ru(bpy)_3]^{2+}$ and the corresponding T_1^{SL} is immeasurably short with our present instrumentation. This effect is expected for the osmium complex due to the greater SOC predicted in that case.

A solvent dependence is also expected for T_1^{SL}. Although the theory of SLR in a glassy matrix is incomplete and little work has been done to quantify glassy solvent effects, it is clear that the details of the phonon structure of the solid matrix are important factors influencing the rate of SLR in paramagnetic species. Equally clear is the fact that the phonon structure is sensitive to the intermolecular interactions within the matrix and that these interactions will be different for different solvents. Therefore, for a range of solvents as diverse as $MeOH/H_2O$ and CH_2Cl_2/Et_2O, that a correlation between solvent and the rate of SLR is found is not unexpected.

In the C_{2v} point group, the spin sublevels of a triplet state are of unique total symmetries, and hence any luminescence that originates from a given sublevel will have polarization at 90° to the polarization of luminescence from either of the other two sublevels. However, intersystem crossing does not typically populate these three sublevels with equal efficiency. Indeed, in many organic systems it is common to find that only a single sublevel is populated predominantly by ISC,[37] producing a significant spin alignment in the excited state if SLR is slow. Population in the remaining sublevels is achieved by the SLR process.

To date, no persuasive explanation of the value obtained for P_{max} in a series of $[Ru(L)_3]^{2+}$ species has been offered. However, the reinterpretation of the TRExP result allows us to make several new conclusions about the nature of the excited states of $[Ru(L)_3]^{2+}$ species.

The observation of a large P approaching the linear–linear limit of 0.5 at any time during the luminescence, such as found in $[Ru(L)_3]^{2+}$ species at t = 0–5 ns, leads to the conclusion that, in that region of excitation (the region of $SSExP_{max}$), absorption is via a *purely* linear oscillator. This also requires that there be no "mixed" absorption, such as that arising from overlapping absorption bands. Any mixed character to the absorption may be shown to have a depolarizing effect upon the luminescence, which will limit the maximum polarization, regardless of the type of emission oscillator. We infer from this (in combination with the nearly identical appearance of the MLCT-bpy absorption bands in the trimer, $[Ru(bpy)_3]^{2+}$, and the monomer, $[Ru(bpy)(py)_4]^{2+}$) that absorption in the region of P_{max} is directly into a localized Ru–bpy chromophore, in agreement with the theoretical analysis of Braterman,[24] with polarization directly along the metal–ligand C_2 axis as proposed for the monomeric complex.

We conclude that the time-dependent decrease of polarization in $[Ru(L)_3]^{2+}$ species is due solely to processes occurring in the lowest triplet state. Furthermore, this state is spatially localized since a near-limiting polarization at t = 0–5 ns following excitation directly into a localized chromophore requires emission from a localized state. For a delocalized state, luminescence would occur in the X–Y plane of the D_3 molecule. However, in the D_3 point group x and y transform as members of a doubly degenerate set, requiring that luminescence polarization occur in the X–Y plane with an arbitrary angle to the X axis. Using the integral method of Albrecht[16] or the equivalent component separation of Carlin,[29] such a delocalized state will produce a $SSExP_{max}$ of $+^1/_7$ and, due to the equivalence of T_X and T_Y (the magnetic sublevels associated with the X and Y axes, respectively), no time dependence in the TRExP experiment.

However, more than one spin sublevel of the triplet state acquires luminescent character for the tris complexes since P_{max} is less than ~0.4. The interpretation that SLR processes are occurring on a nanosecond time scale for these ruthenium complexes is, by itself, insufficient to explain the TRExP result. While slow SLR processes may affect lifetimes and quantum yields, polarization is determined only by the symmetries of those states that dominate the luminescence. It is apparent that, at t = 0–5 ns, the dominant sublevel for a $[Ru(L)_3]^{2+}$ complex is equivalent to the lone luminescent level of the complex $[Ru(bpy)(py)_4]^{2+}$. However, as SLR transfers triplet population into other spin levels, the polarization declines. Although SLR processes occur for the mono-bpy complex, presumably at a rate similar to that of $[Ru(bpy)_3]^{2+}$, the polarization does not fall.[5] The unique property of $[Ru(bpy)_3]^{2+}$ which leads to this "depolarization" lies, therefore, in the fact that, in the trimer system, a triplet level obtains, through some mechanism, luminescent character *which is absent in the case of the monomer.*

The question of how this transition moment arises in the case of the trimer while the monomer exhibits no such moment is of immediate concern. This question will be analyzed more fully, and a model presented, in a separate section below. However, it is possible to explore this problem in a qualitative manner prior to explicit calculation. Radiative moment in the monomer is obtained primarily from spin-allowed charge-transfer transitions between the ground state and singlet states of MLCT configuration by the SOC mechanism. Though, as Kober and Meyer[22] point out, a second substate may couple to the lowest set of ^{1}MLCT states and acquire some luminescent character, the details of the SSExP spectrum reveal that singlet transitions polarized perpendicularly to the C_2 axis of the monomer possess relatively little oscillator strength of their own. Thus little luminescent character will be obtained from that coupling.

In the case of the trimer, $[Ru(L)_3]^{2+}$, there is little change in the intensity and energy of the ^{1}MLCT transitions with respect to the monomer; therefore, this same argument holds true for SOC between spin sublevels of the lowest triplet state in this complex and "internal" localized CT configurations of the excited chromophore. The new feature of the trimer is the presence of other localized chromophores in the complex. These "external" chromophores possess large oscillator strengths to their own ^{1}MLCT manifolds, and polarization of these transitions is along the individual C_2 axes. These "external" C_2 axes are displaced 120° with respect to the "internal" axis system of this discussion, and intensity borrowing is possible between the formerly quiescent internal sublevel and, ultimately, these external transitions.

C. Mixed-Ligand Complexes. In mixed-ligand complexes of the form $[Ru(bpy)(L)_2]^{2+}$ (L = pq and bpz), the maximum SSExP values are of magnitude P_{max} = 0.34. In these complexes, the energy of the π^* orbitals of the L ligands is sufficiently lower than that of the bipyridine ligand that, regardless of excitation wavelength, localization in minima of the lowest surface associated with Ru–L units only will be the result (Figure 9a). This energy gap between the LUMOs of the ligands L and bpy may be such that the lowest surface does not possess any potential minima associated with localization in Ru–bpy luminophores (Figure 9b).

We rationalize the larger $SSExP_{max}$ value generally associated with bis-type complexes in a manner consistent with the concept of interchromophoric coupling, an intensity-borrowing mechanism coupling *localized* triplet transitions with allowed transitions of other chromophores. The reduction in number of external chromophores from the tris complexes reduces the amount of transition intensity available for transfer into the second luminescent triplet sublevel, although not to zero as in the case of the monomeric species. We therefore expect I_z/I_p, the ratio of intensity

(36) Myrick, M. L.; Blakley, R. L.; DeArmond, M. K., unpublished results.
(37) DeGroot, M. S.; Hesselman, I. A. M.; Van der Waals, J. N. *Mol. Phys.* **1967**, *12*(3), 259.

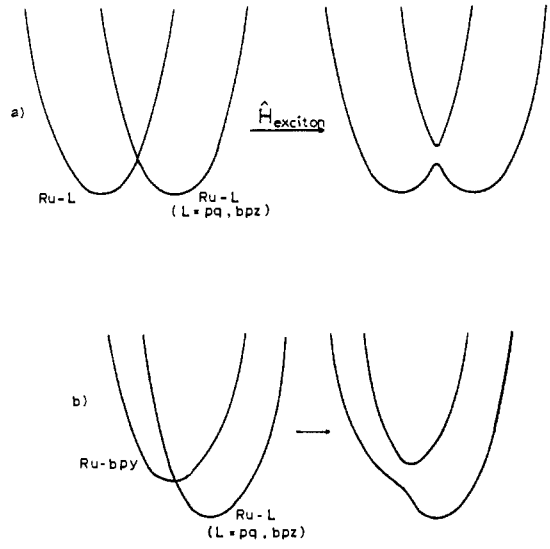

Figure 9. (a) Exciton interaction of two localized Ru–L chromophores in $[Ru(bpy)(L)_2]^{2+}$ (L = pq, bpz). (b) Exciton interaction of localized Ru–bpy and Ru–L chromophores in $[Ru(bpy)_n(L)_{3-n}]^{2+}$ (n = 1, 2) (L = pq, bpz).

polarized along the z axis of the localized unit to that polarized perpendicular to the z axis, will be intermediate between the same ratio for a tris chelate and a mono chelate. Hence the expected value of P_{max} will fall in the range intermediate between 0.23, found for most $[Ru(L)_3]^{2+}$ species, and ~0.5, found for $[Ru(L)(X)_4]^{2+}$ species.

In complexes of the form $[Ru(bpy)_2(L)]^{2+}$ (L = pq, bpz), where the localized transition appears to occur from the Ru–L chromophore and where the CT-L and CT-bpy transitions are well separated in absorption, the $SSExP_{max}$ values found are again near the limiting value of 0.5 and derive from excitation into bands assigned as MLCT-L. These results are rationalized consistent with a model requiring interchromophoric coupling: to a first approximation, no external chromophores are present at low energy to provide significant coupling. Therefore, it is expected that the observed P_{max} value will be approximately the same as found in $[Ru(bpy)(py)_4]^{2+}$. It will be noted in Table I that the P_{max} value in these complexes does exhibit a slightly larger deviation from the limiting value of $+^1/_2$ than the tetrapyridine complex. These slightly lower values, ranging from 0.39 to 0.42, may be attributed to residual interchromophoric coupling between the luminescent localized states and states involving MLCT-bipyridine at much higher energy. In order to test this hypothesis, a TRExP experiment on these complexes is required; however, the SSExP value of ~0.42 is so large that, even assuming a value of 0.45 or 0.46 were obtained in the TRExP of these complexes, the uncertainty in the value would be large enough to make the results questionable. We therefore did not attempt TRExP on these complexes.

D. An Interchromophoric Coupling Model. The purpose of this section is to provide a model to rationalize the results obtained from the photoselection studies. We proceed by first investigating the radiative pathways of the monochelate complex, $[Ru(bpy)(py)_4]^{+2}$, then by applying these results to the bis and tris chelates.

(1) $[Ru(bpy)(py)_4]^{2+}$ and Other Monochelate Species. In this discussion we refer to Figure 10, which shows potential energy surfaces associated with the ground, lowest excited triplet, and general MLCT singlet states. As shown, the lowest triplet consists of three substates with total symmetries A_2, A_1, and B_1 or B_2, such that radiative transitions from these levels are, respectively, forbidden, have z polarized, or have polarized perpendicular to the z axis.

In zeroth order, T_1 has no radiative properties. Rather, it borrows transition moment via SOC from $S_0 \rightarrow S_n$ transitions. The effective integrals have the form

$$\langle \Psi_{S_n} | \lambda L \cdot S | \Psi^{3\alpha}_{T_1} \rangle \qquad (2)$$

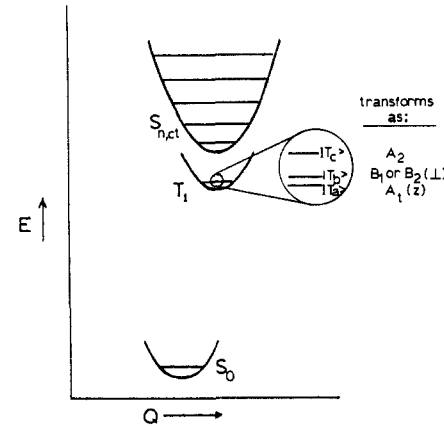

Figure 10. Simplified potential energy surfaces of the monomeric complexes, $[Ru(L)(X)_4]^{2+}$. $S_{n,CT}$ indicates an MLCT singlet excited state, T_1 is the lowest triplet state, and S_0 is the ground state. The zero-field splitting of the lowest triplet level is indicated, and the associated zero-field triplet spin functions are shown.

where α signifies the triplet spin function with principal axis aligned with the α axis. By symmetry,[22] one α state cannot spin–orbit couple, to first order, with any of the available singlet states. The total wave function is given, by first-order perturbation theory (PT), as

$$|\Psi^{3\alpha}_{0,0}\rangle = |\Psi^{3\alpha 0}_{0,0}\rangle + \sum_{\substack{d \\ (d,n,v \neq 3\alpha,0,0)}} \sum_{n} \sum_{v} \frac{\langle \Psi^{d}_{n,v} | \hat{H}_{SO} | \Psi^{3\alpha 0}_{0,0} \rangle}{E^{3\alpha 0}_{0,0} - E^{d}_{n,v}} |\Psi^{d}_{n,v}\rangle \qquad (3)$$

where n ranges over all orbital states, d ranges over all spin functions of the system, and v covers all vibrational levels within the electronic states.

We immediately neglect all coupling via the SOC mechanism to other triplet spin functions due to the negligible radiative properties of those states. Also, we consider only values of n such that MLCT-bipyridine states are considered. This is done because, in general, these are the lowest lying transitions by several thousand cm^{-1}, causing the energy denominator to be large for higher lying states. This reduces the integrals of consideration to

$$|\Psi^{3\alpha}_{0,0}\rangle = |\Psi^{3\alpha 0}_{0,0}\rangle + \sum_{n} \sum_{v} \frac{\langle \Psi^{1}_{n,v} | \hat{H}_{SO} | \Psi^{3\alpha 0}_{0,0} \rangle}{E^{3\alpha 0}_{0,0} - E^{1}_{n,v}} |\Psi^{1}_{n,v}\rangle \qquad (4)$$

For reasons given previously, we may now neglect coupling for the level associated with total symmetry A_2 in Figure 10, rendering it virtually a pure triplet function.

Coupling to electronic and vibronic levels is possible, for the perpendicular polarized $|T_b\rangle$ level (Figure 10), provided the coupling singlet vibronic levels belong to the same irreducible representation as that of this $|T_b\rangle$ level. However, calculation of the transition moment for electric dipole radiation from this level to the ground state (eq 5) gives a radiative moment for this

$$\langle \Psi^{1}_{g} | \hat{\epsilon}_{\perp} | \Psi^{3b}_{0,0} \rangle = \langle \Psi^{1}_{g} | \hat{\epsilon}_{\perp} | \Psi^{3b0}_{0,0} \rangle + \sum_{q} \sum_{r} C^{1}_{qr} \langle \Psi^{1}_{g} | \hat{\epsilon}_{\perp} | \Psi^{1}_{q,r} \rangle \qquad (5)$$

complex that depends upon the transition moments of the $\Psi^1_g \leftarrow \Psi^1_{q,r}$ transitions, where $\Psi^1_{q,r}$ is a vibronic state that can couple to the $|T_b\rangle$ level. The symmetry of the SOC operator requires that these transitions be polarized perpendicularly to the z axis, as indicated by the use of $\hat{\epsilon}_\perp$ as the operator governing the transitions (eq 5). However, the experimental results indicate that most singlet absorbance of MLCT-bipyridine character is z polarized. Hence, this sublevel is also nearly radiation silent in the mono complex.

Only the triplet level associated with $|T_a\rangle$, with total symmetry A_1, attains a nonnegligible radiative property via our approximate SOC treatment. This level is connected to the ground state by $\hat{\epsilon}_z$, and the singlet wave functions to which it couples possess large transitions moments to Ψ^1_g.

From this point the discussion is concerned with the bis chelates, utilizing some of the results obtained for the monomeric species.

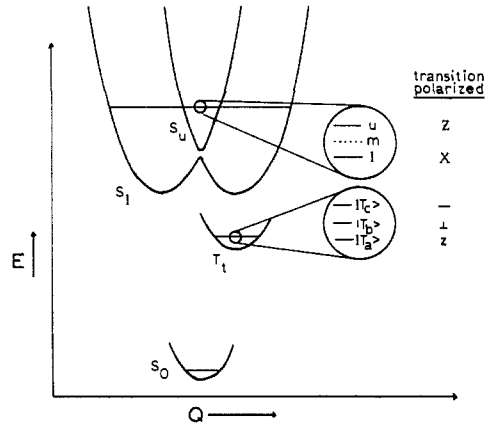

Figure 11. Simplified potential energy surfaces of the dimeric species, $[Ru(L)_2(X)_2]^{2+}$. S_l and S_u are lower and upper singlet surfaces, respectively, of ^{1}MLCT configuration. T_l is a localized triplet minimum. The upper exploded view shows the splitting of a single monomer level into dimer levels with polarization along the overall dimer axes.

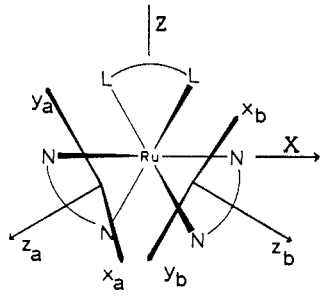

Figure 12. Axis systems of dimer (X, Y, Z) and individual monomer (x, y, z) units. Monomer systems are identical with those of Figure 8. Ru is the only atom lying in the plane of the paper.

(2) $[Ru(bpy)_2(X)_2]^{2+}$ and Related Bis Chelates. The discussion in the following paragraphs will involve information given in Figures 11 and 12 about the shape of the excited-state manifold and appropriate axis systems for the two limiting cases of the dimer, localized and delocalized.

To zeroth order, T_l, a localized triplet function, has no inherent radiative properties but borrows intensity from spin-allowed transitions via SOC.

Using an equation of the form of eq 3, we can neglect coupling of the emitting triplet to other triplet states and concentrate only on coupling to ^{1}MLCT-bipyridine states. Furthermore, we restrict our consideration to the only singlet 0–0 transition to carry any intensity in the case of the monomer. That is, we assume this transition to be the identical transition in the dimer. We neglect the z-polarized vibronic transitions originating from silent 0–0 modes for the time being. These require the involvement of non-totally symmetry vibrations, for which there is no evidence in the resonance Raman spectra of the dimer and trimer species.[38] In effect, we assume that only a single ^{1}MLCT-bipyridine transition and its vibronic satellites appear in the absorbance of this bis complex.

The new feature present for the bis complex in the very weak exciton coupling scheme is the presence of a delocalized excited singlet state at slightly higher energy than the localized excited singlets, as described by Braterman[24] in a discussion of the trimer. Here then is the key feature that induces mixed polarization: A delocalized level occurs with a large transition probability to the ground state, and this chromophore also possesses significant electronic overlap with the localized chromophore.

Note that the lowest surface of the charge-transfer singlet state of this discussion possesses a second minimum indicative of localization in the second chromophore. This minimum also possesses radiative moments, but due to the negligible electronic

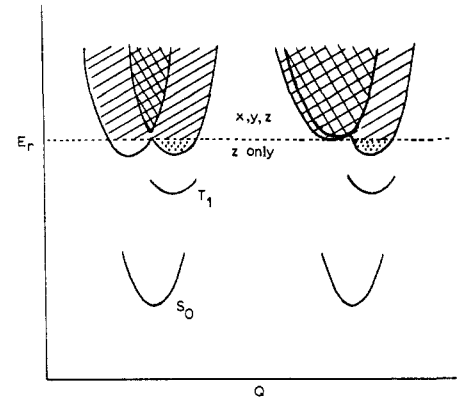

Figure 13. Potential energy surfaces of the dimer and trimer species showing major regions of interaction with the localized triplet. E_r is the energy of the top of the barrier between localized singlet minima. The stipled area below E_r is the region of localized interaction, while the hatched area above E_r indicates the region of delocalized interaction.

(as well as vibrational) interaction between this localized level and the localized triplet under consideration, no coupling is induced from the localized ^{1}MLCT state of another chromophore to the lowest levels of the first chromophore. This may be demonstrated by calculation of SOC, using localized states of the Kober and Meyer[22] description, between a general singlet and general triplet localized on separate chromophores. Ignoring vibrational overlap, this analysis yields terms of the type shown below:

$$\langle(\pi_1^*)(\sigma)|\hat{H}_{SO}|(\pi_2^*)(\sigma)\rangle\langle(d)|(d)\rangle\langle(\sigma)|(\sigma)\rangle \quad (6a)$$

$$\langle(\pi_1^*)(\sigma)|\hat{H}_{SO}|(d)(\sigma)\rangle\langle(d)|(\pi_2^*)\rangle\langle(\sigma)|(\sigma)\rangle \quad (6b)$$

$$\langle(d)(\sigma)|\hat{H}_{SO}|(d)(\sigma)\rangle\langle(\pi_1^*)|(\pi_2^*)\rangle\langle(\sigma)|(\sigma)\rangle \quad (6c)$$

where π_a^* indicates a π^* orbital localized on the ath ligand, σ indicates a one-electron spin function, d indicates the vacant d orbital of the CT configuration, and H_{SO} is the one-electron SOC operator, $\lambda L(1)\cdot S(1)$. Due to the negligible overlap of π_1^* and π_2^*, each of these terms becomes insignificant.

To proceed, we make a few simplifying approximations consistent with experimental evidence.

(1) We assume exciton splitting to be small in the singlet manifold. This is reasonable due to the apparent absence of excitonic energy effects on the ^{1}MLCT and ^{3}MLCT transitions.

(2) We assume that, up to the level of the maximum in the lowest singlet surface, all excitation is directly into localized states. Alternatively, this may be expressed by requiring that inversion doubling of vibrational levels below this maximum is negligible.[39]

(3) We assume that, above this maximum in the lower singlet surface, excitation of the singlet is directly into delocalized levels with polarization given by exciton theory.

Therefore, using first-order PT, we may express the lowest level of the localized triplet in a form such as

$$\Psi_{0,0}^{3\alpha} = \Psi_{0,0}^{3\alpha 0} + (\text{coupling to } \Psi^1 \text{ of } E < E_r) + (\text{coupling to } \Psi^1 \text{ of } E > E_r) \quad (7)$$

where E_r is the energy of the central maximum of the lowest surface. By inspection of the diagram in Figure 11, the coupling of the localized triplet to the localized region of the singlet state is seen to be the coupling present in the monomer to states below the energy E_r for a hypothetical monomer with zero-point energy of the allowed singlet equal to that of the dimer.

Hence we expect that, for levels below E_r, coupling will be only to the triplet level transforming as z in the monomer and will be that of the monomer.

The third term of eq 7 is more difficult to analyze, but may, however, be divided into two portions. The first of these will deal with coupling of the triplet to delocalized levels of the lowest singlet surface, while the second connects the localized triplet to delo-

(38) Angel, S. M.; DeArmond, M. K.; Donohoe, R. J.; Wertz, D. W. *J. Phys. Chem.* **1985**, *89*, 282.

(39) Herzberg, G. *Electronic Spectra of Polyatomic Molecules*; Van Nostrand: New York, 1945.

calized levels of the upper singlet surface (Figure 13). Exciton theory predicts the polarization of transitions to these levels of the singlet manifold to be directed along the overall molecular axes, Z, X, Y, indicated in Figure 12.

We may therefore use eq 7 in the form

$$\Psi^{3\alpha}_{0,0} = \Psi^{3\alpha 0}_{0,0} + \delta_{\alpha,a}\sum_{l,v<E_r} K^m_v \Psi^1_{l,v} + \sum_{l,v>E_r}\frac{H^{\alpha}_{l,v}}{\Delta E_{TS}}\Psi^1_{l,v} + \sum_{u,v}\frac{H^{\alpha}_{u,v}}{\Delta E_{TS}}\Psi^1_{u,v} \quad (8)$$

where $H_{k,v} = \langle \Psi^1_{k,v}|\hat{H}_{SO}|\Psi\alpha bv3\alpha 0_{0,0}\rangle$, $\Delta E_{TS} = E^3_{k,v} \approx E^{3\alpha 0}_{0,0} - E^1_{k,v}$, α is a spin index, $\delta_{\alpha,a} = 1$ if $\alpha = a$, 0 if $\alpha \neq a$, and K^m_v = coupling coefficient of monomer to l,v level.

The delocalized levels of the lower singlet surface are expected, by exciton theory, to have polarizations along the X molecular axis indicated in the diagram, and the delocalized levels of the upper singlet surface are expected to produce polarizations along the Z molecular axis.[40] Since these levels are not quantized along the localized axes, they are expected to couple with the z triplet sublevel as well as the perpendicular sublevel, either x or y, of the monomer.

At this point we must distinguish two possibilities. The lowest triplet state must not be of the same orbital configuration as the absorbing singlet state; however, this leaves two MLCT configurations to choose from. The first is an MLCT state of $\mathbf{B}_1$ orbital symmetry. If this state is lowest in energy, sublevels occur that may luminesce with polarization along the monomer z and y axes. If, however, the state that is of orbital B_2 symmetry is lowest in energy, then polarization along the monomer z and x axes is possible. Because x and y of the monomer differ in the extent of their orthogonality with the overall Z and X axes, different degrees of polarization are possible depending upon which state lies at lowest energy. Hence we treat these possibilities separately.

In Table II are listed the nine distinct angles between the chosen axis systems of the dimer and monomer. The actual axis systems of these moieties are expected to be slightly displaced from the positions indicated in Figure 12 due to the low symmetry of the species involved; however, they should be close to the systems given there, and we use these to calculate approximate values for the true complex system.

Exciton theory predicts the polarization of delocalized transition from levels associated with the upper surface to be polarized along the Z dimer axis. Given a totally symmetric ground state, this implies a level that transforms with Z in the C_{2v} point group. To obtain the extent of SOC coupling to triplet levels of symmetry x, y, and z of the monomer, we obtain the projection of Z on each of these axes and recall that, if the axes coincide, the total SOC integral would equal $(1/2^{1/2})H_{SO,m}$, where $1/2^{1/2}$ is derived from the participation of the monomer level in the delocalized level and m indicates that $H_{SO,m}$ is the value of coupling between the triplet state of the monomer and the singlet monomer level from which the delocalized level derives. This gives eq 9a–f.

$$H^z_{l,v} = \frac{\cos X_z}{2^{1/2}}H_{SO,m} \quad (9a)$$

$$H^x_{l,v} = \frac{\cos X_x}{2^{1/2}}H_{SO,m} \quad (9b)$$

$$H^y_{l,v} = \frac{\cos X_y}{2^{1/2}}H_{SO,m} \quad (9c)$$

$$H^x_{u,v} = \frac{\cos Z_z}{2^{1/2}}H_{SO,m} \quad (9d)$$

$$H^x_{u,v} = \frac{\cos Z_x}{2^{1/2}}H_{SO,m} \quad (9e)$$

$$H^y_{u,v} = \frac{\cos Z_y}{2^{1/2}}H_{SO,m} \quad (9f)$$

(40) Kasha, M.; Rawls, H. R.; Asnraf El-Bayoumi, M. *Pure Appl. Chem.* **1965**, *11*, 371.

Inclusion of this result simplifies eq 8 to the form

$$\Psi^{3\alpha}_{0,0} = \Psi^{3\alpha 0}_{0,0} + \delta_{\alpha,z}\sum_{l,v<E_r} K^M_v \Psi^1_{l,v} + \frac{\cos\theta_1(\alpha)}{2^{1/2}}\sum_{l,v>E_r}\frac{H_{SO,M}}{\Delta E_{TS}}\Psi^1_{l,v} + \frac{\cos\theta_2(\alpha)}{2^{1/2}}\sum_{u,v}\frac{H_{SO,M}}{\Delta E_{TS}}\Psi^1_{u,v} \quad (10)$$

We proceed to calculation of the singlet–triplet transition moment between the lowest triplet states and the ground state of the dimer, finding

$$\langle S_0|\hat{\epsilon}|\Psi^{3\alpha}_{0,0}\rangle = \langle S_0|\hat{\epsilon}(\alpha)|\Psi^{3\alpha}_{0,0}\rangle = \langle S_0|\hat{\epsilon}(\alpha)|\Psi^{3\alpha 0}_{0,0}\rangle + \delta_{\alpha,a}\sum_{l,v<E_r} K^M_v\langle S_0|\hat{\epsilon}(\alpha)|\Psi^1_{l,v}\rangle + \frac{\cos\theta_1(\alpha)}{2^{1/2}}\sum_{l,v>E_r}\frac{H_{SO,M}\langle S_0|\hat{\epsilon}(\alpha)|\Psi^1_{l,v}\rangle}{\Delta E_{TS}} + \frac{\cos\theta_2(\alpha)}{2^{1/2}}\sum_{u,v}\frac{H_{SO,M}\langle S_0|\hat{\epsilon}(\alpha)|\Psi^1_{u,v}\rangle}{\Delta E_{TS}} \quad (11)$$

The first term on the right side of eq 11 reduces to zero in all cases, the second term appears in only the case of $\alpha = a$, and the remaining terms contribute disproportionately to $\alpha = a$ and $\alpha = b$. Evaluation as far as possible to this point gives the transition moments for the α transitions, M_z (for $\alpha = a$) and $M_\perp$ (for $\alpha = b$), as

$$M_z = K_M + \left[\frac{\cos X_z}{2^{1/2}}\sum_{l,v>E_r}\frac{H_{SO,M}M^{l,0}_z}{\Delta E_{TS}} + \frac{\cos Z_z}{2^{1/2}}\sum_{u,v}\frac{H_{SO,M}M^{u,0}_z}{\Delta E_{TS}}\right] \quad (12a)$$

$$M_\perp = \left[\frac{\cos\theta_1(\alpha)}{2^{1/2}}\sum_{l,v>E_r}\frac{H_{SO,M}M^{l,0}_\perp}{\Delta E_{TS}} + \frac{\cos\theta_2(\alpha)}{2^{1/2}}\sum_{u,v}\frac{H_{SO,M}M^{u,0}_1}{\Delta E_{TS}}\right] \quad (12b)$$

Note that the transition moments appearing in eq 12a and 12b are not the pure transition moments of the delocalized levels, but are the transition moments in the z, x, y directions induced by a transition of the delocalized chromophore. Again we make use of the angles in Table I in this evaluation. Exciton theory predicts the total transition moments of the Z and X dimer levels to be $(1/2^{1/2})M_m$ and $(3/2)^{1/2}M_m$, respectively, where M_m is the transition moment of the monomeric level from which the delocalized level is formed. We therefore summarize the transition moments along the monomer axes as in eq 13a–f.

$$M^{l,0}_z = {}^1/_2(\cos X_z)M_m \quad (13a)$$

$$M^{u,0}_z = \frac{\cos Z_z}{2^{1/2}}M_m \quad (13b)$$

$$M^{l,0}_y = {}^1/_2(\cos X_y)M_m \quad (13c)$$

$$M^{u,0}_y = \frac{\cos Z_y}{2^{1/2}}M_m \quad (13d)$$

$$M^{l,0}_x = {}^1/_2(\cos X_x)M_m \quad (13e)$$

$$M^{u,0}_x = \frac{\cos Z_x}{2^{1/2}}M_m \quad (13f)$$

Inserting these definitions into eq 12a and 12b, we simplify this to the forms of eq 14a and 14b.

$$M_z = K_m + \frac{3^{1/2}\cos^2 X_z}{2}\sum_{l,v>E_r}\frac{H_{SO,m}M_m}{\Delta E_{TS}} + \frac{\cos^2 Z_z}{2}\sum_{u,v}\frac{H_{SO,m}M_m}{\Delta E_{TS}} \quad (14a)$$

$$M_\perp = \frac{3^{1/2}\cos^2\theta_1(\alpha)}{2}\sum_{l,v>E_r}\frac{H_{SO,m}M_m}{\Delta E_{TS}} + \frac{\cos^2\theta_2(\alpha)}{2}\sum_{u,v}\frac{H_{SO,m}M_m}{\Delta E_{TS}} \quad (14b)$$

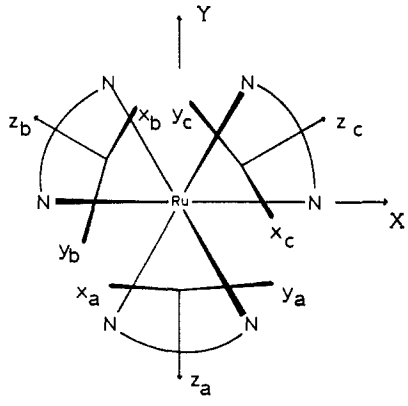

Figure 14. Axis sytems of trimer (X, Y, Z) and individual monomer (x, y, z) units. Monomer systems are identical with those of Figure 8. Ru is the only atom lying in the plane of the paper.

The forms shown in eq 14a and 14b may be further simplified by combining left and right summations. This makes use of the assumption that the excitonic splitting of the singlet levels is negligibly small, such that ΔE_{TS}, the energy separation from a given triplet sublevel to a given vibronic level of the excited singlet manifold, is virtually identical for upper and lower levels derived from the same monomer function. Therefore we combine the summations and index them only by energy, omitting l or u in the description of the levels. This produces eq 15a and 15b.

$$M_z = K_m + \left(\frac{\cos^2 Z_z + 3^{1/2} \cos^2 X_z}{2} \right) B \qquad (15a)$$

$$M_\perp = \left(\frac{\cos^2 \theta_2(\alpha) + 3^{1/2} \cos^2 \theta_2(\alpha)}{2} \right) B \qquad (15b)$$

$$B = \sum_{E>E_r} \frac{H_{SO,m} M_m}{\Delta E_{TS}}$$

We now extend these results to the tris-chelate complexes.

(3) $[Ru(bpy)_3]^{2+}$ and Related Tris Chelates. For this discussion, we refer to the diagrams shown in Figures 14 and 15, showing the monomer and trimer axis systems and the potential energy surfaces produced via very weak exciton coupling.

Again, the triplet levels may be represented in the form

$$\Psi^{3\alpha}_{0,0} = \Psi^{3\alpha 0}_{0,0} + \delta_{\alpha,a} \sum_{l,v<E_r} K^M_v \Psi_{l,v} + \sum_{l,v>E_r} \frac{H^\alpha_{l,v}}{\Delta E_{TS}} \Psi^1_{l,v} + \sum_{u,v} \frac{H^\alpha_{u,v}}{\Delta E_{TS}} \Psi^1_{u,v} \qquad (16)$$

where $H^\alpha_{k,v} = \langle \Psi^1_{k,v} | \hat{H}_{SO} | \Psi^{3\alpha 0}_{0,0} \rangle$, $\Delta E_{TS} = E^3_{u,v} - E^{3\alpha 0}_{u,v} - E^1_{k,v}$, $\delta_{\alpha,a} = 1$ if $\alpha = a$, 0 if $\alpha = b$ and cpK^M_v = coupling coefficient of monomer to l,v level.

The same choice is made for the orientation of the triplet level which carries polarization perpendicular to z.

We need not consider the higher energy delocalized singlet surface because it does not possess any radiative character (to first order) due to the excitonic interactions that produce it. Therefore, we need only consider interactions between a localized triplet and the two lowest surfaces of the singlet manifold above it.

The middle surface of the singlet manifold does possess minima, as Braterman[24] has pointed out. However, they are shallow and we ignore them.

The integrals $H_{k,v}$ are evaluated in the same manner as for the dimer with two differences. The root mean square contribution of the monomer single wave function to any of the delocalized wave functions is $1/3^{1/2}$; also, we must at some point take into account the fact that, due to the degeneracy of X and Y in the D_3 point group, the X and Y axes may occur arbitrarily in the X,Y plane. The latter point is held in abeyance momentarily so that we may proceed to the result below.

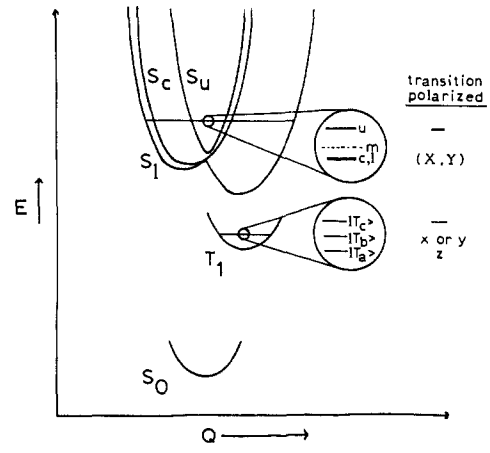

Figure 15. Simplified potential energy surfaces of the trimeric species, $[Ru(L)_3]^{2+}$. S_l, S_c, and S_u are lower, central, and upper singlet surfaces, respectively, of ^{1}MLCT configuration. T_1 is a localized triplet minimum. The upper exploded view shows the splitting of a single monomer level into trimer levels with polarization along the overall trimer axes.

$$H^z_{l,0} = \frac{\cos X_z}{3^{1/2}} H_{SO,m} \qquad (17a)$$

$$H^z_{u,0} = \frac{\cos Y_z}{3^{1/2}} H_{SO,m} \qquad (17b)$$

$$H^y_{l,0} = \frac{\cos X_y}{3^{1/2}} H_{SO,m} \qquad (17c)$$

$$H^y_{u,0} = \frac{\cos Y_y}{3^{1/2}} H_{SO,m} \qquad (17d)$$

$$H^x_{l,0} = \frac{\cos X_x}{3^{1/2}} H_{SO,m} \qquad (17e)$$

$$H^x_{u,0} = \frac{\cos X_y}{3^{1/2}} H_{SO,m} \qquad (17f)$$

We then write eq 16 as

$$\Psi^{3\alpha}_{0,0} = \Psi^{3\alpha 0}_{0,0} + \delta_{\alpha,a} \sum_{l,v<E_r} K^M_v \Psi^1_{l,v} + \frac{\cos \theta_2(\alpha)}{3^{1/2}} \sum_{l,v>E_r} \frac{H_{SO,m}}{\Delta E_{TS}} \Psi^1_{l,v} + \frac{\cos \theta_2(\alpha)}{3^{1/2}} \sum_{u,v} \frac{H_{SO,m}}{\Delta E_{TS}} \Psi^1_{u,v} \qquad (18)$$

where u indicates a level arising from the central surface, and l indicates levels arising from the lowest surface of the trimer.

Proceeding to calculation of the transition moment for the localized triplet level, we find

$$\langle S_0|\hat{\epsilon}|\Psi^{3\alpha}_{0,0}\rangle = \langle S_0|\hat{\epsilon}(\alpha)|\Psi^{3\alpha}_{0,0}\rangle = \langle S_0|\hat{\epsilon}(\alpha)|\Psi^{3\alpha 0}_{0,0}\rangle + \delta_{\alpha,a} \sum_{E<E_r} K^M_v \langle S_0|\hat{\epsilon}(\alpha)|\Psi^1_{l,v}\rangle + \frac{\cos \theta(\alpha)}{3^{1/2}} \sum_{E>E_r} \frac{H_{SO,m} \langle S_0|\hat{\epsilon}(\alpha)|\Psi|^1_{l,v}\rangle}{\Delta E_{TS}} + \frac{\cos \theta(\alpha)}{3^{1/2}} \sum_{E>E_r} \frac{H_{SO,m} \langle S_0|\hat{\epsilon}(\alpha)|\Psi^1_{u,v}\rangle}{\Delta E_{TS}} \qquad (19)$$

Again the first term is zero in all cases and the second appears only for $\alpha = a$. Evaluation now leads to

$$M_z = K_m + \left[\frac{\cos X_z}{3^{1/2}} \sum_{E>E_r} \frac{H_{SO,m} M^{l,0}_z}{\Delta E_{TS}} + \frac{\cos Y_z}{3^{1/2}} \sum_{E>E_r} \frac{H_{SO,m} M^{u,0}_z}{\Delta E_{TS}} \right] \qquad (20a)$$

$$M_\perp = \left[\frac{\cos\theta_1(\alpha)}{3^{1/3}} \sum_{E>E_r} \frac{H_{SO,m} M_\perp^{l,0}}{\Delta E_{TS}} + \frac{\cos\theta_2(\alpha)}{3^{1/2}} \sum_{E>E_r} \frac{H_{SO,m} M_\perp^{u,0}}{\Delta E_{TS}} \right] \quad (20b)$$

where z indicates the monomeric z axis, $\perp$ indicates either the x or y monomer axis, $H_{SO,m}$ is the SOC between the corresponding levels of the monomer, M_b is the transition moment induced in the b direction by transitions from k,v to the ground state, and $\Delta E_{TS} = E^3_{0,0} - E^1_{l,v} \approx E^{3\alpha 0}_{0,0} - E^1_{l,v}$.

As for the dimer, we interpret the transition moments shown in eq 20a and 20b in terms of the monomeric transition moments by referring to Table III. The total transition moments along the X and Y trimer axes are $(3/2)^{1/2}M_m$ and $(3/2)^{1/2}M_m$, respectively, and we find

$$M_z^{l,0} = \frac{3^{1/2}\cos X_z}{2^{1/2}} M_m \quad (21a)$$

$$M_z^{u,0} = \frac{3^{1/2}\cos Y_z}{2^{1/2}} M_m \quad (21b)$$

$$M_y^{l,0} = \frac{3^{1/2}\cos X_y}{2^{1/2}} M_m \quad (21c)$$

$$M_y^{u,0} = \frac{3^{1/2}\cos Y_y}{2^{1/2}} M_m \quad (21d)$$

$$M_x^{l,0} = \frac{3^{1/2}\cos X_x}{2^{1/2}} M_m \quad (21e)$$

$$M_x^{u,0} = \frac{3^{1/2}\cos Y_x}{2^{1/2}} M_m \quad (21f)$$

where the letter m again indicates the value for the free monomeric transition. We reduce eq 20a and 20b to

$$M_z = K_m + \frac{1}{2^{1/2}} B \quad (22a)$$

$$M_\perp = \frac{\cos^2\theta_1(\alpha) + \cos^2\theta_2(\alpha)}{2^{1/2}} B \quad (22b)$$

$$B = \sum_{E>E_r} \frac{H_{SO,m} M_m}{\Delta E_{TS}}$$

At this point we must account for the arbitrary nature of the X and Y axes in the plane which they define. This is now easily done by noting

$$\cos^2\theta_1(\alpha) + \cos^2\theta_2(\alpha) + \cos^2\theta_3(\alpha) = 1 \quad (23)$$

where θ_1 is the angle between the monomer axis of consideration and the trimer X axis, θ_2 is the angle to the trimer Y axis, and θ_3 is the angle to the trimer Z axis. We may replace the sum of the first two terms of eq 23 by $1 - \cos^2\theta_3(\alpha)$, which is invariant. Table III lists the angles between the axes of Figure 14, as well as average angles, average cosines, and average squares of cosines of interest in the trimer.

(4) Results of Calculations. To summarize the values of the transition moments of the spin levels, we find for the dimer

$$M_z = K_m + 0.7745B \quad (24a)$$

$$M_y = 0.1793B \quad (24b)$$

$$M_x = 0.3944B \quad (24c)$$

$$B = \sum_{E>E_r} \frac{H_{SO,m} M_m}{\Delta E_{TS}}$$

The corresponding equations for the trimeric complex are

$$M_z = K_m + 0.7071B \quad (25a)$$

$$M_y = 0.3339B \quad (25b)$$

$$M_x = 0.6661B \quad (25c)$$

$$B = \sum_{E>E_r} \frac{H_{SO,m} M_m}{\Delta E_{TS}}$$

(5) Polarization Effects Predicted by the ICC Model. Carlin and DeArmond[2a] have produced a form of the polarization equation convenient for the interpretation of the theoretical results of the ICC model which is reproduced as eq 26.

$$P = [(2A - B - C)a + (-A + 2B - C)b + (-A - B + 2C)c]/[(4A + 3B + 3C)a + (3A + 4B + 3C)b + (3A + 3B + 4C)c] \quad (26)$$

where the absorption oscillator is described by

$$\hat{A} = A_x + B_y + C_z \quad (27)$$

and the emission oscillator by

$$\hat{E} = a\hat{x} + b\hat{y} + c\hat{z} \quad (28)$$

Note that ABC and abc are proportional to the oscillator strengths in the x, y, and z directions. For our discussion, we see that the absorption oscillator carries intensity only in the z monomer direction for excitation on the red edge of absorbance (in the region of P_{max}) for the tris and bis complexes and through the entire absorbance of the monomer. Therefore, we set $A = B = 0$.

In the event that the B_1 state is lowest in energy, transitions are possible of z and y polarization. This is represented by setting $a = 0$. For the B_2 state lowest, z and x polarizations are possible and we set $b = 0$ to reflect this. Equation 26 leads to the following forms for each possibility, respectively.

$$P = \frac{-b + 2c}{3b + 4c} \quad (29a)$$

$$P = \frac{-a + 2c}{3a + 4c} \quad (29b)$$

Upon substitution of the extreme values for a or b, the transition moment along the perpendicular axis, and c, the moment along the z axis, the limiting values for the ICC model result.

For the pure monomer, $a = b = 0$ and the predicted polarization is $+^1/_2$. No other value is possible since mixed polarization is impossible for this Ru(II) species.

Table IV lists the predicted limiting values for mono, bis, and tris chelates predicted by this model for both possibilities of lowest state symmetries (note that we rule out A_1 as the lowest triplet orbital symmetry due to the large negative polarization expected in that case).

The experimental value of P_{max} for tris chelates is approximately 0.23 (with the exception of $[Ru(biq)_3]^{2+}$), and therefore the ratio a/c or b/c must be 0.639. This is inconsistent with emission from the B_1 triplet state, is likely from the B_2 state, and leads to the conclusion that the ratio K/B is 0.1261 for the trimer. If we assume this ratio remains constant from the trimer to the normal bis species, we calculate the a/c ratio for a bis complex to be approximately 0.192. Therefore, we would predict a P_{max} value for a normal bis complex to be approximately 0.39.

Experimentally, most bis-type complexes produce values of $P_{max} \approx 0.34$, demonstrating a reasonable correlation between the predictions of this model and experiment. The experimental shortfall is explicable in terms of partial failure of some assumptions of the model. In particular, we neglect any overlap of delocalized singlet absorbance with the localized absorbance on the red edge.

Note from the results of Table I that $[Ru(biq)_3]^{2+}$ provides an exception to the general rule that tris chelate complexes give P_{max} of 0.23. The reasons for the unusually large $P_{max} \approx 0.38$ of $[Ru(biq)_3]^{2+}$ are uncertain at present, but at least three possibilities exist consistent with the ICC model. $[Ru(biq)_3]^{2+}$ is slightly

Table III. Angles (Deg) between Trimer and Monomer Axes (of Figure 14)

angle	value	$(\|\cos\|)_{av}$[a]	$(\cos^2)_{av}$[a]
Z,x	54.7	0.578	0.334
Z,y	35.3	0.816	0.667
Z,z	90	0	0
X,x	144.6	0.520	0.333
X,y	54.7	0.368	0.167
X,z	90	0.637	0.500
Y,x	90	0.520	0.333
Y,y	90	0.368	0.167
Y,z	0	0.637	0.500

[a] Averaged over all orientations of X and Y axes in X,Y plane.

Table IV

complex	emitting orbital state	oscillators	limiting values of P_{max} max	min
monomer	B_1	z	0.5	0.5
	B_2	z	0.5	0.5
dimer	B_1	z; x	0.5	0.36
	B_2	z; y	0.5	0.46
trimer	B_1	z; x	0.5	0.17
	B_2	z; y	0.5	0.38

photosensitive, and the possibility remains that the high polarization results from an excited state in which partial dissociation is occurring, reducing the molecule to an effective bis or mono complex. A second rationale lies in differences in Franck–Condon overlap factors between excited states and the ground state for this sterically hindered complex, possibly indicated by the unusual band shape of the ^{1}MLCT absorbance. This would certainly affect the coupling relationships between localized triplet states and the singlet manifold, as well as possibly affecting the barrier height between localized moieties, resulting in shifts in the ratio K/B for this species.

A third rationale lies in a rearrangement of energy levels for this bulky complex, causing the B_1 level to fall lowest in energy for the complex. If K/B remained similar to that of the tris-bipyridine species, this would result in $P_{max} \approx 0.41$.

Summary

The similarity of emission, absorption, and excitation photoselection spectra for monomeric Ru–bpy to that of the bis and tris complexes of this unit as well as the anomalous excitation photoselection (SSExP) value in the singlet charge-transfer region has enabled the emitting excited state for all of these complexes to be characterized as a spatially isolated localized transition; this is a process characteristic of the Ru–bpy chromophore. The decrease in magnitude of the P_{max} for the bis ($P_{max} \sim 0.34$) and tris ($P_{max} \sim 0.23$) complexes from the linear absorber–linear emitter limit (0.5) of the monomeric Ru–bpy is a critical detail in the proper description of the excited-state behavior for this unusual emitters. The absence of solvent dependence for the polarization spectra and the measurement in rigid media indicate that the reduction in P and the mechanism of localization are not of environmental origin. The recognition that a time-dependent decrease in P_{max} for the tris complexes from the linear–linear limit (0.5) to the steady-state values measured is not due to localized exciton hopping but is a spin–lattice relaxation among the spin states of the localized orbital triplet enables presentation of an appropriate model. For the C_{2v} monomer unit Ru–bpy in $[Ru(bpy)(py)_4]^{2+}$ experimental polarization indicates that the spin-forbidden emission borrows intensity only from the z-polarized singlet charge-transfer state and no other spin state carries significant intensity. Consequently, the occurrence of spin–lattice relaxation in the bis and tris complexes to the other two spin states indicates that these spin levels have acquired intensity by a mechanism not present in the monomer complex. This process can be identified as an "interchromophoric" coupling; that is the $Ru(bpy)_3^{2+}$ complex utilizes the two additional Ru–bpy chromophores to introduce intensity components perpendicular to the monomer z axis. Utilizing standard perturbation theory with appropriate spin–orbit matrix elements, coupling between the localized triplet and the localized portion of the singlet (as in the monomer) as well as the delocalized portions of the singlet (Figure 15) enables quantitative evaluation of the polarization in these complexes. (Note that the mechanism does not require interligand spin–orbit coupling.)

Consequently, the anomalous P occurring on the red edge side of the charge-transfer band in the bis and tris complexes does arise from the same localized transition that occurs in the monomer complex, $[Ru(bpy)(py)_4]^{2+}$. The 0.1 P values measured at higher energy in the singlet charge-transfer absorption result from absorption to the delocalized (D_3) charge-transfer portion of the singlet and subsequent emission from the localized (C_{2v}) and triplet with mixed polarization.

The question of the number of emitting electronic states occurring for these Ru^{II} complexes must now be answered. This and the extension of this model of the emission behavior and polarization spectra for the Os^{II} diimine complexes will be the topics of future publications.

Acknowledgment. This work was supported by a grant from the Army Research Office (Grant No. DAAL-03-86-K-0040).

Registry No. $[Ru(bpy)(py)_4]^{2+}$, 47779-68-0; $[Ru(bpy)_3]^{2+}$, 15158-62-0; $[Ru(phen)_3]^{2+}$, 22873-66-1; $[Ru(bpz)_3]^{2+}$, 75523-96-5; $[Ru(pq)_3]^{2+}$, 60451-53-8; $[Ru(biq)_3]^{2+}$, 60451-55-0; $[Ru(bpy)_2(phen)]^{2+}$, 22563-13-9; $[Ru(bpy)(phen)_2]^{2+}$, 22563-12-8; $[Ru(bpy)_2(bpz)]^{2+}$, 85335-53-1; $[Ru(bpy)(bpz)_2]^{2+}$, 85335-51-9; $[Ru(bpy)_2(pq)]^{2+}$, 74171-82-7; $[Ru(bpy)(pq)_2]^{2+}$, 74171-83-8.